PEER-REVIEWED ARTICLE bioresources.cnr.ncsu.edu

Effects of Chitin Nano-flake Fillers on the Mechanical and Barrier Properties of Polylactic Acid Biocomposite Films

Soojin Kwon,[a] Sang Yun Kim,[b] Kyudeok Oh,[b,c] and Jung Soo Han [d,*]

Polylactic acid (PLA) is a biodegradable polymer extensively used in packaging; however, its mechanical and barrier properties require enhancement for wider applications. Chitin-derived nanoflakes (CNFL), a two-dimensionally separated nanomaterial derived from α-chitin, possess high strength and toughness, making them ideal additives for improved PLA performance. This study investigated the effect of CNFL on the properties of PLA composite films. Incorporating CNFL significantly enhanced the mechanical properties of PLA, increasing its tensile strength and stiffness while preserving flexibility. This enhancement was attributed to the nucleating effect of CNFL, which increases crystallinity. Additionally, CNFL improved the thermal stability of the composite films by mitigating thermal deformation. Notably, the oxygen barrier properties of CNFL-filled PLA composites were also enhanced, demonstrating a significant reduction in oxygen permeability at optimal CNFL concentrations due to increased tortuosity of the oxygen diffusion path. Overall, CNFL-filled PLA composites exhibit great potential as renewable packaging materials, particularly for protecting sensitive products, such as food and pharmaceuticals, from oxidative degradation, thereby extending shelf life and maintaining quality. These findings suggest that CNFL-filled PLA composites are promising materials for advanced applications, offering a combination of enhanced mechanical performance, improved thermal stability, and superior oxygen barrier properties.

DOI: 10.15376.biores.19.4.7216-7238

Keywords: Biocomposites; Chitin; Nanomaterials; Oxygen barrier; Polylactic acid; 2D material

*Contact information: a: Department of Chemical & Biomolecular Engineering, University of Delaware, Newark, DE, 19716, USA; b: Program in Environmental Materials Science, Department of Agriculture, Forestry and Bioresources, College of Agriculture and Life Sciences, Seoul National University, Seoul, 08826, South Korea; c: Research Institute of Agriculture and Life Science, Seoul National University, Seoul 08826, South Korea; d: Department of Biobased Materials, Chungnam National University, 99 Daehak-ro, Yuseong- gu, Daejeon, 34134, South Korea; *Corresponding author: han1606@cnu.ac.kr*

INTRODUCTION

The increasing consumption of plastic and the accumulation of its waste on our planet have raised serious concerns about our environment and ecosystems. With the convenience of its production and usage, approximately 10,000 Mt of plastic had been produced as of 2017, and 7,000 Mt had become waste, primarily landfilled (Geyer 2020a,b). Considering the recalcitrant nature of plastic waste and the continued increase in plastic production, it is projected that accumulated plastic waste will reach 33,000 Mt by 2050. Substantial efforts have been made to reduce plastic waste and replace plastic products.

Bio-based plastics, also known as bioplastics, use renewable resources and have the potential to replace synthetic, fossil-based plastics. Bioplastics have been extensively researched regarding their performance and sustainability. For example, bio-based polyesters such as polylactic acid (PLA), polyhydroxyalkanoate, and polybutylene succinate have been reported as biodegradable and renewable bioplastics. However, their mechanical properties, such as brittleness, still require improvement to compete with their fossil-based counterparts (Cao *et al.* 2019; Z. Naser *et al.* 2021).

Compositing with filler materials is one of the simplest and most cost-effective ways to enhance the mechanical properties of polymers (Wootthikanokkhan *et al.* 2013; Yadav *et al.* 2023; Jani *et al.* 2024). Especially with natural fillers, this method offers advantages such as improved biodegradability and reduced environmental impact (Korol *et al.* 2016; Civancik-Uslu *et al.* 2018; Mahmoud Zaghloul *et al.* 2021; Kane *et al.* 2022; Kumar *et al.* 2022). For example, cellulose nanofibrils, lignin, and starch have been used to reinforce PLA (Lezak *et al.* 2008; Wootthikanokkhan *et al.* 2013; Battegazzore *et al.* 2014; Fiore *et al.* 2014; Joseph Arockiam *et al.* 2022). In general, natural fillers enhance the tensile modulus and elasticity of PLA, but they often exhibit reduced tensile strength compared with neat PLA (Hubbe and Grigsby 2020; Hubbe *et al.* 2021).

A crucial consideration when compositing fillers with bioplastics is the compatibility between the two materials. Bioplastics such as PLA exhibit hydrophobic properties, whereas many natural fillers (*e.g.*, cellulose and starch) are hydrophilic. This disparity hinders uniform mixing and can result in poor mechanical properties. Therefore, adjusting the hydrophobicity/hydrophilicity of fillers is essential to enhance compatibility with the polymer matrix.

Chitin is produced through the chemical treatment of shellfish waste, such as crab and shrimp shells. Based on the large volume of shellfish waste generated globally (FAO 2014; Yan and Chen 2015), chitin is considered the second most abundant biopolymer after cellulose. Chitin possesses several superior properties, such as high strength and toughness (Ravi Kumar 2000; Wei *et al.* 2021). Additionally, the hydrophobic nature of chitin, particularly α-chitin (Francesko *et al.* 2010; Islam *et al.* 2024), offers great potential for improved compatibility with hydrophobic PLA polymer matrices.

Chitin inherently possesses complex hierarchical structures (Nikolov *et al.* 2011; Hou *et al.* 2021). At the molecular level, chitin consists of N-acetylglucosamine units that form polymer chains, aligning and creating microfibrils through hydrogen bonding. These microfibrils aggregate into fibril bundles, which further form larger chitin-protein complexes with a thickness of 20 nm (Nikolov *et al.* 2011). These complexes create a multilayered bulk cuticle structure, the main component of the protective layer in shellfish. During the purification of chitin using alkaline and acid treatments, proteins and minerals are removed, leaving only chitin fibrils in this Bouligand structure (Aklog *et al.* 2016). This hierarchical arrangement is maintained even after treatment.

The hierarchical structure of chitin allows it to be utilized in various dimensions and scales, from the nanoscale to the micro- and macro-scales, depending on the intended purpose. Numerous studies have investigated the disintegration/fibrillation of chitin structures to produce nanochitin for nanoscale applications (Bai *et al.* 2022). Most research has focused on nanochitin in the form of nanofibers (Fan *et al.* 2010; Lu *et al.* 2013; Tanaka *et al.* 2014) and nanocrystals (Oun and Rhim 2018; Liu *et al.* 2020; Yuan *et al.* 2020; Fernández-Marín *et al.* 2024), which require harsh mechanical or chemical treatment. Recently, it was reported that cellulose can be separated into a two-dimensional form when a non-polar solvent is used with ball-milling (Zhang *et al.* 2020). Considering the

multilayered structure of chitin, it was expected that this process could also be applied to prepare two-dimensional chitin nanomaterial, suitable for application in manufacturing. While the typical method for chitin nanomaterial production requires organic acids such as acetic acid, the current method using the ball-milling process with only recoverable volatile solvents indicates a more sustainable and cost-effective approach.

Reinforcing PLA with chitin materials has been studied by various researchers (Zhang *et al.* 2014; Nasrin *et al.* 2017; Hassan and Koyama 2020). These studies showed that incorporating chitin into PLA resulted in lower water absorptivity, enhanced tensile strength and stiffness, and antimicrobial properties. However, the loading amount of chitin was limited to 3 to 4% due to a decrease in tensile strength and lower thermal stability beyond this point. Additionally, most studies focused on using chitin as nanocrystals or micron-scale powder.

This study focused on two-dimensionally separated, disc-type nanochitin, specifically chitin-derived nanoflakes (CNFL). Disc-type nanofillers offer advantages in terms of enhancing mechanical, barrier, and thermal properties, as well as facilitating strong interactions with polymers (Hatta *et al.* 1992; Shen *et al.* 2021; Gao *et al.* 2023). Particularly, various disc or plate-type fillers have been used to enhance gas, oxygen, and moisture barriers by increasing tortuosity in porous structures, thereby hindering the penetration and passage of oxygen or moisture through films (Yu *et al.* 2013; Cui *et al.* 2015; Tan and Thomas 2016; Lee *et al.* 2018). Additionally, their high aspect ratio and large surface area can improve the mechanical properties of composites through enhanced interaction with the polymer matrix (Kumar Patel and Purohit 2019; Karim *et al.* 2021; Kiziltas *et al.* 2021; Usman *et al.* 2022; Gao *et al.* 2023).

A previous study demonstrated that chitin microparticles can be effectively compatibilized with PLA, yielding stronger, stiffer, and more elastic biocomposites (Han *et al.* 2024). In this study, chitin was nanosized further to CNFL, and its benefits as a filler for PLA biocomposites was investigated, focusing on the mechanical and barrier properties. The biocomposites introduced in this study are valuable for their renewability—they are entirely biomass-derived—and for addressing the limitations of previous biocomposites. The authors anticipate that these biocomposites can be further developed into environmentally friendly, safe, and cost-effective materials for oxygen barriers.

EXPERIMENTAL

Materials

α-Chitin powder from crab shell was purchased from Amicogen (Seoul, South Korea) for CNFL preparation. PLA pellets (4032D, $M_w \approx 1{,}950$ kg/mol) was purchased from NatureWorks (Plymouth, MN, USA). The chemicals, including chloroform and n-heptane, were purchased as EP grade from Samchun Chemicals (Seoul, South Korea). All materials and solvents were used as received without further purification.

Preparation of CNFL

CNFL was prepared by ball-milling treatment using an Attrition mill (KMDC-1B, Korea Machine Engineering, Korea). Twenty grams of α-chitin powder was added to a zirconium jar, followed by 266 g of n-heptane. One kilogram of zirconia balls (diameter: 3 mm) was added, and the milling was conducted at 200 rpm, maintaining a temperature of approximately 20 °C. After milling, the n-heptane was decanted, and the milled samples

were dried at 80 °C for 8 h. The milled samples were designated as 2h, 4h, 12h, and 24h, based on the milling duration.

Preparation of CNFL-filled PLA Composite Films

Neat PLA and CNFL-filled composite films were prepared using the solvent-casting method. Initially, 10 g of PLA powder was added to 90 g of chloroform with gentle stirring for 2 h at room temperature to obtain a 10 wt% PLA solution. For CNFL-filled samples, the desired amounts of PLA and CNFL-4h were added to 90 g of chloroform (60.4 mL) to achieve PLA solutions with varying CNFL loading ratios (0.1, 0.5, 1, 3, and 5 wt%). For homogeneous dispersion, the solution was stirred for 24 h. All other conditions remained consistent. Each PLA solution was poured onto a glass plate and spread using a doctor blade to form a 50-µm-thick film. The solvent was allowed to evaporate overnight, and the films were then vacuum-dried at 80 °C overnight to ensure complete removal of any residual chloroform. The resulting composite films were designated according to their CNFL loading ratios: 0.1%, 0.5%, 1%, 3%, and 5%.

Characterization of Prepared CNFL

The characteristics of the prepared CNFL were analyzed in comparison to the pristine chitin powder, focusing on the degree of substitution, crystalline and chemical structures, and particle morphologies.

Elemental analysis of the pristine chitin powder and prepared CNFL was conducted using an automatic elemental analyzer (Flash 2000, Thermo Fisher Scientific, Waltham, MA, USA). The acetyl group content was characterized by the degree of substitution (DS), calculated using Eq. 1 (Ifuku *et al.* 2010),

$$(C/12.01) / (N/14.01) = (6 + 2\chi) / 1 \quad (1)$$

where C and N are the weight percentages of carbon and nitrogen, respectively, and χ is the DS value of the acetyl groups.

X-ray diffraction (XRD) patterns of the samples were obtained using an X-ray diffractometer (D8 DISCOVER, Bruker AXS, Karlsruhe, Germany) with a Cu-Kα radiation source at 40 kV, 40 mA, 2θ = 5° to 50°, a divergence angle of 0.2°, and a step size of 0.02. The crystallinity was calculated in accordance with the methodology described by Yuan *et al.* (2011). The crystallite sizes of the (0 2 0), (1 1 0), and (1 2 0) planes were derived from deconvoluted XRD data. The full width at half maximum (FWHM) of each peak was measured, and crystallite sizes (τ) were calculated using the Scherrer equation (Goodrich and Winter 2007),

$$\tau = \frac{0.9\lambda}{\beta cos\theta} \quad (2)$$

where τ is the mean size of crystallite, λ is the X-ray wavelength, β is the FWHM, and θ is the Bragg angle.

Attenuated total reflectance-Fourier transform infrared spectroscopy (ATR-FTIR) was performed to characterize the chemical structure of the samples. ATR-FTIR spectra were recorded on a Nicolet Nexus 670 (Thermo Electron Corporation, Waltham, MA, USA), equipped with a KRS-5 crystal (refractive index: 2.4) and using an incidence angle of 45°. The spectra were recorded in transmittance mode over the wavenumber range of 650 to 4000 cm^{-1}, with a resolution of 4 cm^{-1}, and after 128 scan accumulations.

The morphologies of the pristine chitin and CNFL were analyzed using field

emission-scanning electron microscopy (FE-SEM; S-4800, Hitachi, Tokyo, Japan) with an accelerating voltage of 5 to 10 kV. A droplet of 0.01 w/v% of the diluted sample/water suspension was deposited on a silicon wafer, air-dried, and then coated with platinum. To measure the thickness of CNFL, atomic force microscopy (AFM) imaging was performed using a scanning probe microscope (XE-100, PSIA, Sungnam, Korea) non-contact mode with a frequency of 300 kHz The sample for AFM was prepared using the same method as described for SEM, excluding the platinum coating.

Thermogravimetric analysis (TGA; STA 449 F5 Jupiter, NETZSCH, Selb, Germany) was performed to assess the thermal stability of chitin and CNFL. The analysis was conducted over a temperature range of 20 °C to 800 °C, with a heating rate of 10 °C/min.

Characterization of CNFL-filled PLA Composite Films

Thermogravimetric analysis and differential scanning calorimetry (DSC; DSC 204 F1 Phoenix, NETZSCH) of the films were performed under a nitrogen atmosphere. Approximately 3 mg of the samples were used for both TGA and DSC analyses. TGA was conducted from 25 to 800 °C, with a heating rate of 10°C/min. DSC analysis was conducted after removing the thermal history of the samples, in accordance with the ASTM method (ASTM D3418 2021). Briefly, the sample was initially heated from 20 to 200 °C at a heating rate of 20 °C/min, held isothermal for 3 min, then cooled to −60 °C at the same rate and held isothermal for 1 min. During the third scan, DSC data were collected from −60 to 200 °C. The crystallinity of the films was calculated using Eq. 3 (Shakoor and Thomas 2014; Zhang *et al.* 2014),

$$\chi_c = \frac{\Delta H_m - \Delta H_{cc}}{\omega \Delta H_m^*} \times 100 \, , \quad (3)$$

where χ_c is the crystallinity (%), ω is the weight fraction of PLA in the composite films, $\Delta H_m$is the measured heat of fusion, ΔH_{cc} is the measured enthalpy of cold crystallization, and ΔH_m^* is the heat of fusion of 100% crystalline PLA (93 J/g) (Martin and Avérous 2001; Shakoor and Thomas 2014).

The mechanical properties of the prepared films were analyzed using a universal tensile testing machine (UTM; Micro 350, Testometric Co., Ltd., Lancashire, UK), following ASTM D882 (2018), except for the sample length. The samples were cut into strips of 10 mm × 60 mm and held under controlled humidity and temperature conditions (50% RH and 23 °C, respectively) overnight before testing. The gauge length was 30 mm, and the test speed was 10 mm/min. The thickness of each sample was measured using a micrometer (L&W Micrometer, Lorentzen & Wettre, Kista, Sweden), and the density of each film (g/cm³) was calculated from its basis weight (g/m²) divided by its thickness (μm). The viscoelasticity of the composite films was analyzed with a dynamic mechanical analyzer (TGA/DSC1, Mettler Toledo, OH, USA). The sample was heated from 27 to 200 °C at a heating rate of 3 °C/min, with a frequency of 1 Hz.

A thermal mechanical analyzer (TMA Q400, TA Instruments, New Castle, DE, USA) was used to analyze volumetric changes in the samples with increasing temperature. The composite films were cut to dimensions of 5 mm × 6 cm and measured under 0.05 N of tension from −20 to 150 °C, with a heating rate of 5 °C/min. The dimensional change of the test film was measured, and the linear coefficient of thermal expansion (LCTE; ppm/°C) was calculated by dividing the value by the temperature range and the original test span of the film (15 mm). The LCTE was measured before and after the glass transition

temperature (T_g) of the composite films.

The oxygen barrier properties of the biocomposite films were investigated by measuring the oxygen transmission rate. Oxygen transmission rates ($cm^3/m^2/day$) of the films were measured using an ultra-precision oxygen analyzer (OX-TRAN Model 2, MOCON, Brooklyn Park, MN, USA) at 23 °C, 1 atm, and 0% RH for 1 day, in accordance with ASTM D3985 (2017). The samples were measured without a mask, and the oxygen permeated through the samples from the oxygen chamber to the chamber purged with nitrogen was measured. The nitrogen carrier gas contained hydrogen at 2%, and the oxygen test gas contained 100 % oxygen. To adjust for variations in film thickness, the oxygen permeability ($cm^3\mu m/m^2/day/atm$) was calculated *via* multiplication of the measured oxygen transmission rate by the film thickness.

RESULTS AND DISCUSSION

CNFL Characteristics

The morphologies and structures of chitin and CNFL were investigated using elemental analysis and microscopic images obtained through SEM and AFM evaluations, as shown in Fig. 1. Because CNFL was only mechanically treated with chitin, its elemental composition and degree of substitution (DS) remained unchanged from that of chitin, confirming their analogous chemical structures (Table 1).

Table 1. Elemental Composition and Degree of Acetyl Group Substitution of Chitin and CNFL

	C (wt.%)*	N (wt.%)**	DS***
α-Chitin	42.53	6.24	0.98
CNFL (24h)	41.6	6.05	0.98

CNFL: chitin-derived nanoflake/s, * Carbon weight percent, ** Nitrogen weight percent, *** Degree of acetyl group substitution, DS

The hierarchical structure of chitin was confirmed in the SEM images (Fig. 1). As mentioned in the Introduction section, chitin is composed of a Bouligand structure with 20-nm-thick layers, which consist of chitin fibrils, proteins, and minerals (Nikolov *et al.* 2011). The layered structure in a chitin flake can be observed, and the chitin fibrils comprising these layers are visible in the magnified images shown in Fig. 1.

Through the ball-milling process, flake-like materials were obtained from chitin. The size of the chitin flakes noticeably decreased with increasing ball-milling time, as shown in the SEM images of CNFL-2h, -4h, and -12h. After 12 h of treatment, the CNFL appeared sufficiently delaminated, with minimal change observed thereafter. These flakes exhibited varying widths but were very thin, with thicknesses under 5 nm (cf. AFM images in Fig. 1). Therefore, these nanoflakes were designated CNFL. Considering that a single microfibril sheet in the laminated structure of natural chitin is approximately 20 nm thick (Nikolov *et al.* 2011), these flakes were likely further delaminated to become thinner than a single microfibril sheet.

Mechanical treatments, including grinding and ball-milling, are typical methods that can efficiently disintegrate the chitin structure into one-dimensional nanofibrils (Ifuku *et al.* 2011; Tran *et al.* 2019). Notably, all of these studies were performed in hydrophilic environments, including polar solvents such as water or N,N-dimethylformamide (DMF).

Recently, it was demonstrated that mechanical treatments of cellulose in a hydrophobic environment using low or non-polar solvents produce 2D cellulose sheets at the nanoscale (Zhao *et al.* 2016; Zhang *et al.* 2020). Because low or non-polar solvents can only permeate the interface between the hydrophobic crystalline faces of cellulose, unlike water, mechanical milling can exfoliate nanoscale cellulose sheets consisting of the hydrophobic crystalline surface (Zhang *et al.* 2020).

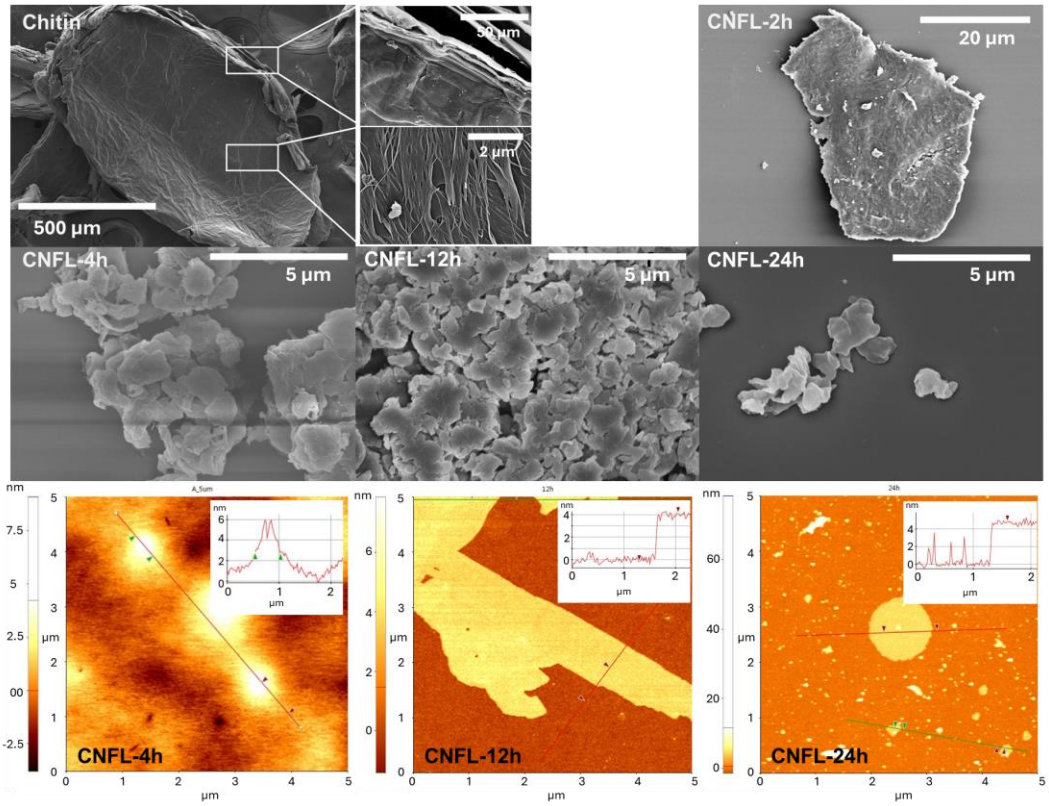

Fig. 1. Morphologies of chitin and chitin-derived nanoflake/s (CNFL). Scanning electron microscopy images of chitin and CNFL, and atomic force microscopy images of CNFL

In this study, n-heptane was used as the exfoliating solvent. It is considered non-polar due to its very low dielectric constant (ε_r) of 1.92 at 20 °C, which facilitates the exfoliation of 2D CNFL from chitin. Additionally, n-heptane has a boiling point of 98.42 °C, making it suitable for solvent recovery by evaporation after CNFL production. Typically, one-dimensional (*i.e.* fibrillar) chitin nanofibrils are produced with the aid of organic acids such as acetic acid. However, this method requires only volatile solvents, not organic acids, making it a more cost-effective and environmentally friendly process.

There was a substantial size difference between chitin and CNFL. CNFLs are small, with widths of less than 10 µm (Fig. 1); the width of each chitin layer is 0.5 to 1 mm. According to the mechanism of other 2D nanomaterial processes (Yi *et al.* 2013), ball-milling generates force on chitin in two ways: shear force, parallel to the chitin sheet, which primarily exfoliates the CNFL; and collision or vertical force, which fragments large sheets into smaller sheets and can sometimes destroy crystalline structures. Considering the much smaller width of CNFL compared with chitin flakes, CNFL was more affected by vertical force than by shear force in this study. To obtain larger CNFLs, the vertical force should be minimized by adjusting processing parameters such as ball size and milling speed.

The change in the crystalline structure of CNFL was investigated using XRD, as shown in Fig. 2. Chitin and chitin nanofibrils exhibited three characteristic peaks at 2θ = 9.5°, 19.2°, and 20.6°, indexed as (0 2 0), (1 1 0), and (1 2 0), respectively (Fan *et al.* 2010). With ball-milling treatment, the crystalline peaks became less distinct, and the XRD patterns resembled an amorphous hump, which was more prominent for CNFL-12h and CNFL-24h samples. This was also confirmed by the decreased crystallinity with increased ball-milling time, calculated from the XRD spectra (from 83% to 33%). Furthermore, the crystallite sizes of the (0 2 0), (1 1 0), and (1 2 0) planes decreased from 7.67, 5.66, and 6.67 nm to 2.12, 1.18, and 2.36 nm, respectively, with the exfoliation of CNFL from chitin. This indicates that mechanical treatment with ball-milling not only delaminates the chitin layers but also disrupts the crystalline structure of chitin.

The decrease in CNFL crystallinity is attributed to damage to the crystalline structure of chitin during ball-milling (Tran *et al.* 2019; Zhang *et al.* 2020). In the case of cellulose, ball-milling with non-polar solvents results in a decreased crystallite size of the (2 0 0) plane, indicating the presence of hydrophobic crystalline surfaces (Zhang *et al.* 2020). The authors explained that the non-polar solvent may preferentially interact with the hydrophobic (2 0 0) crystalline surfaces, weakening the interactions between the crystal planes, thereby producing 2D cellulose nanosheets exposed on the (2 0 0) surfaces (Zhang *et al.* 2020). Similarly, in the case of α-chitin, the interaction between the hydrophobic crystalline surfaces appears to be weakened by ball-milling with n-heptane. This is demonstrated by the decreased crystallite size of the (1 1 0) and (1 2 0) planes, which are the hydrophobic crystalline planes of chitin (Ogawa *et al.* 2010).

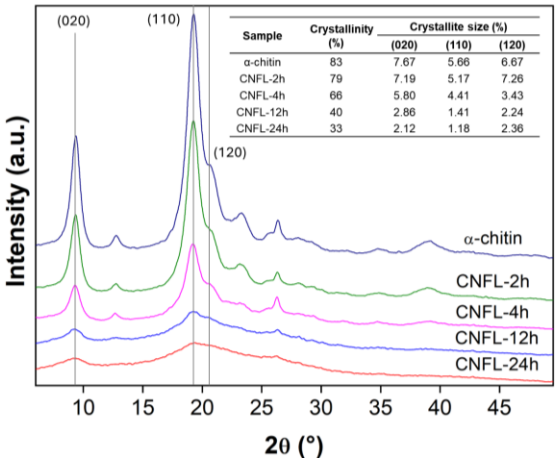

Sample	Crystallinity (%)	Crystallite size (%) (020)	(110)	(120)
α-chitin	83	7.67	5.66	6.67
CNFL-2h	79	7.19	5.17	7.26
CNFL-4h	66	5.80	4.41	3.43
CNFL-12h	40	2.86	1.41	2.24
CNFL-24h	33	2.12	1.18	2.36

Fig. 2. X-ray diffraction patterns, crystallinity, and crystallite sizes in the (020), (110), and (120) planes of chitin and CNFL with different ball-milling treatment times (2, 4, 12, and 24 h).

The FTIR analysis of chitin and CNFL, as shown in Fig. 3, confirmed the weakening of interactions between the crystal planes. Chitin and CNFL exhibited different absorbance peak heights at several wavelengths. Although chitin displayed sharp peaks, most peaks in CNFL showed lower absorbance, and some peaks disappeared. In the FTIR spectrum of α-chitin, the doublet peaks at 1656 and 1627 cm^{-1} are attributed to the amide I band, which is sensitive to hydrogen bonding and indicates the crystalline structure of α-chitin (Cárdenas *et al.* 2004; Ogawa *et al.* 2010; Hasegawa 2017). After 12 h of ball-milling, the split of the peaks became less distinct (Fig. 3 (b)), and the FTIR spectrum of CNFL resembled that of β-chitin (Cárdenas *et al.* 2004), suggesting a transition from a planar crystalline structure to a more loosened crystalline structure (Hou *et al.* 2021).

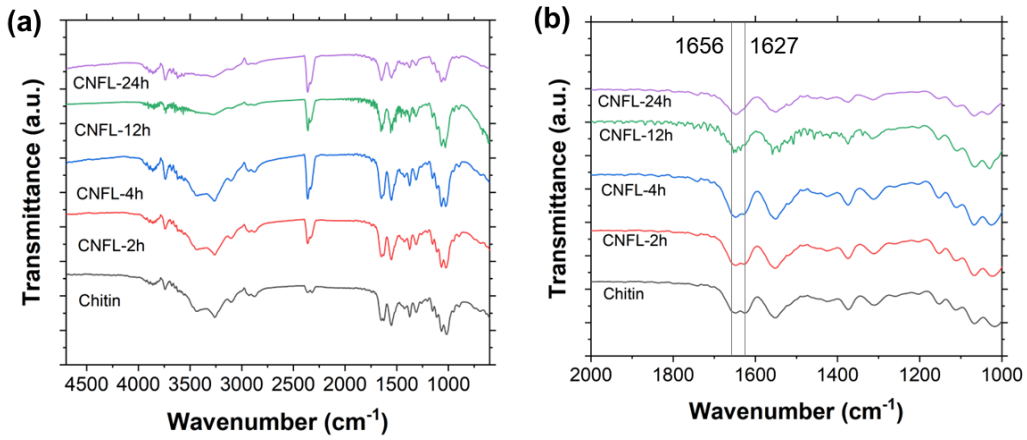

Fig. 3. FTIR spectra of chitin and CNFL with different ball-milling treatment times (2, 4, 12, and 24 h)

The interpretation of the 1656 and 1627 cm^{-1} peaks is controversial; however, there is a consensus regarding (1) the peak at 1656 cm^{-1}, indicating hydrogen bonding between the carbonyl group and the amino group (C=O···H-N) either within the same chain (Cárdenas *et al.* 2004) or between neighboring chains in the same sheet (Focher *et al.* 1992; Rinaudo 2006; Dahmane *et al.* 2014), and (2) the peak at 1627 cm^{-1}, which may represent the hydrogen bond of the carbonyl group to the hydroxymethyl group, either within the same chain (Focher *et al.* 1992; Rinaudo 2006; Dahmane *et al.* 2014), between different chains in the same sheet (Cárdenas *et al.* 2004; Hasan *et al.* 2022), or between different sheets. Thus, the 1627 cm^{-1} peak reflects the chemical stability of the chitin chains/structures. Consequently, a decrease in the 1627 cm^{-1} peak in CNFL suggests a reduction in the number of hydrogen bonds (C=O···H-N) stabilizing the crystalline structure of α-chitin, due to the milling treatment (Kameda *et al.* 2005) (Deconvoluted peaks are shown in Fig. A1 in Appendix). This assumption is consistent with the reduced thermal stability of CNFL relative to chitin, as shown in the TGA analysis (Fig. A2).

Characteristics of CNFL-filled PLA Composite Films

The characteristics of CNFL-filled PLA composite films were investigated with respect to their mechanical, thermal, and oxygen barrier properties.

Mechanical properties of CNFL-filled PLA composite films

The tensile properties of the composite films were enhanced by incorporating CNFL (Fig. 4 and Fig. A3). In Fig. 4(a), the tensile stress of the composite films exhibited an increasing trend with increasing amounts of CNFL, indicating the positive effect of CNFL on the tensile strength of the composite. Similar to tensile stress, Young's modulus also increased with the addition of CNFL (Fig. 4(b)). The tensile stress significantly increased at 5% CNFL concentration, which differs from the reduction in tensile strength observed at over 3% chitin microparticle concentration in the previous study (Hassan and Koyama 2020). Young's modulus reflects the material's stiffness, where higher values indicate greater stiffness. The maximum increase was observed at a 5% CNFL concentration, with Young's modulus reaching 2.8 GPa, a 75% improvement over pure PLA. This suggests that the CNFL-filled PLA composite films became both stronger and stiffer with increasing CNFL content. These enhancements could be attributed to better stress transfer and improved interaction between the PLA matrix and the CNFL.

The viscoelastic properties of the composite films were further investigated using dynamic mechanical analysis (DMA), with a focus on the storage modulus and loss tangent, as shown in Fig. 4(c) and (d). The storage modulus increased with the addition of CNFL in the temperature range below T_g, indicating increased stiffness and greater capacity to store elastic energy in the composite films. The loss tangent results aligned with the storage modulus findings. Overall, the loss tangent decreased with increasing CNFL content, suggesting enhanced elasticity and reduced viscosity in the composite films. In Fig. 4(d), the peak temperature of the loss tangent indicates the T_g of the composite films. Despite the overall increase in modulus with CNFL addition, the T_g of the composite slightly decreased upon CNFL addition, implying a plasticizing effect of CNFL on PLA. Additionally, the reduced T_g suggests that flexibility, ductility, and/or impact resistance can be improved by CNFL addition. However, considering that a lower loss tangent indicates less energy dissipation, the brittleness of the composite films may require further improvement, which could be a direction for future research.

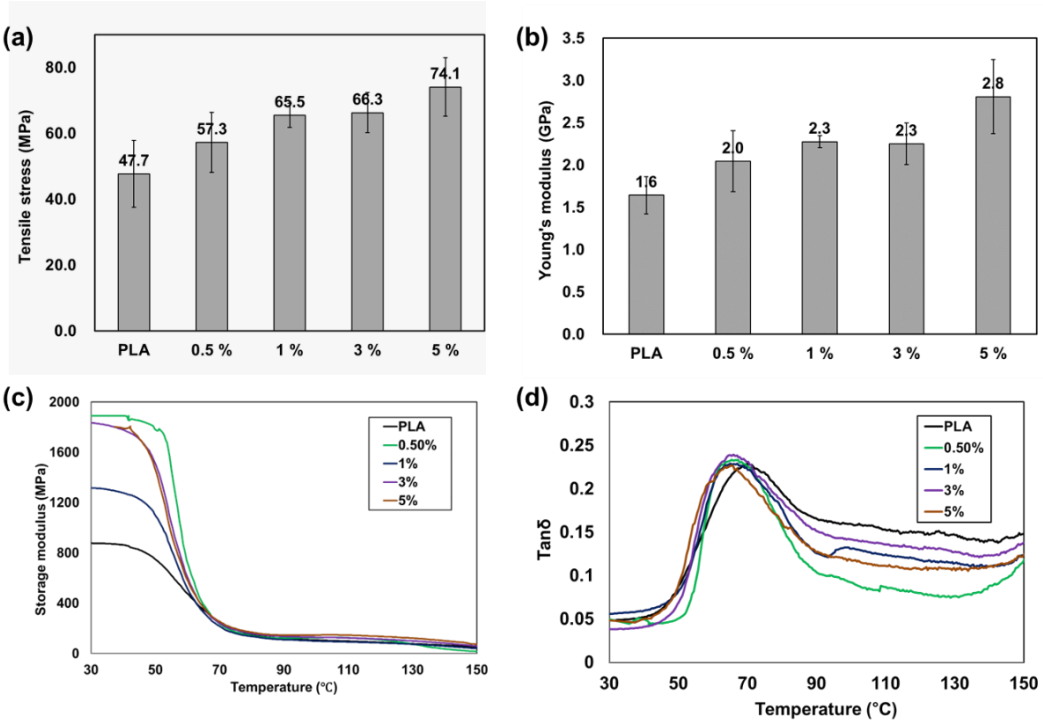

Fig. 4. Mechanical properties of CNFL-filled polylactic acid (PLA) composites with CNFL loading ratios of 0.1%, 0.5%, 1%, 3%, and 5%. Tensile properties of the composite films: (a) tensile stress and (b) Young's modulus. Viscoelastic properties of the composite films: (c) storage modulus and (d) loss tangent (tangent delta; tanδ) measured by dynamic mechanical analysis

Thermal properties of CNFL-filled PLA composite films

The thermal properties of CNFL-filled PLA composite films were investigated using DSC and TGA, as illustrated in Fig. 5. The heat of fusion and crystallinity of PLA in the composite films were measured and calculated based on the DSC results (Fig. 5(a) and Table 2).

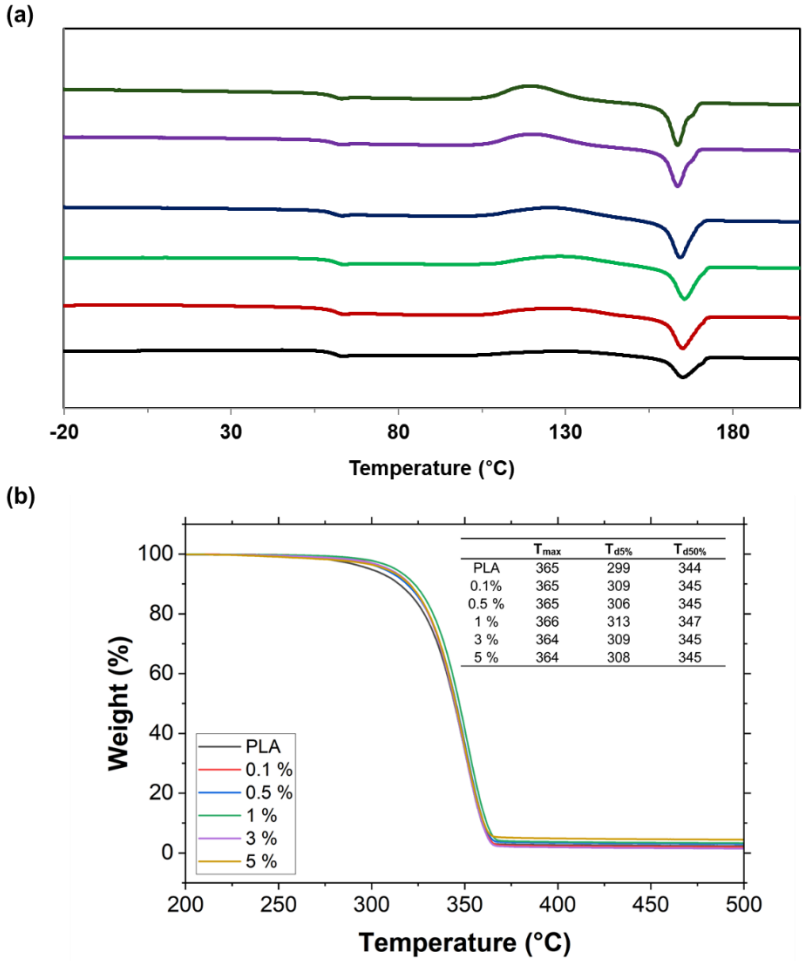

Fig. 5. Differential scanning calorimetry (a) and thermogravimetric analysis (b) curves of CNFL-filled PLA composite films with CNFL loading ratios of 0.1%, 0.5%, 1%, 3%, and 5%. T_{max}: maximum degradation temperature from the peak temperature of the derivative curves of TGA; $T_{d5\%}$: initial degradation temperature at 5% weight loss; and $T_{d50\%}$: degradation temperature at 50% weight loss.

The crystallinity of PLA in the composites decreased with CNFL addition. However, this decrease was not significant, considering the initially low crystallinity of PLA. Cold crystallization was observed near 110 to 130 °C and increased with higher CNFL content. This result suggests that further treatment, such as thermal processing, could control cold crystallization and thereby modulate the mechanical properties (Lizundia *et al.* 2013). The increased cold crystallization could be attributed to the nucleating effect of CNFL on PLA crystallization, which is supported by reports of nucleating effects of fillers in composites (Papageorgiou *et al.* 2010; Shakoor and Thomas 2014; Ouchiar *et al.* 2016; Zhang *et al.* 2022). CNFL may improve the mobility of PLA polymer chains, facilitating the rearrangement of crystalline structures and promoting cold crystallization, which could contribute to the ductility and flexibility of the composites. Additionally, well-dispersed CNFL in the PLA matrix likely facilitated the uniform formation of crystalline structures.

The T_g measured by DSC showed no significant differences across the different CNFL addition conditions, whereas the T_g in the tanδ curve exhibited a decreasing trend with increasing CNFL content. This discrepancy could be attributed to the different heating

rates used in DMA (3 °C/min) and DSC (20 °C/min) measurements. Moreover, DMA utilizes frequency-dependent measurements, causing T_g to vary according to the specific conditions used. DMA is more sensitive to changes in mechanical properties; thus, the observed decrease in T_g in DMA suggests increased chain mobility under mechanical stress, potentially due to the plasticizing effect of CNFL. Considering the higher measurement sensitivity of DMA to changes in viscoelastic properties (Foreman *et al.* 2011), DSC might not detect subtle changes in the composites.

Table 2. Thermal Properties and Crystallinity of CNFL-filled PLA Composite Films Measured by DSC

	T_g (°C)	T_{cc} (°C)	T_m (°C)	ΔH_{cc} (J/g)	ΔH_m (J/g)	CrI (%)
PLA	60	129	164.97	20.3	23.2	3.2
CNFL 0.1 %	60	127	164.95	28.3	32.4	4.5
CNFL 0.5 %	60	129	165.46	31.4	33.6	2.4
CNFL 1 %	60	126	164.27	35.6	36.8	1.3
CNFL 3 %	60	121	163.44	36.7	36.3	0
CNFL 5 %	60	120	163.44	38.2	38.2	0

Notes: T_g: glass transition temperature; T_{cc}: cold crystallization temperature; T_m: melting temperature; CrI: crystallinity of the composite films calculated based on the heat of fusion (ΔH_m) and the enthalpy of cold crystallization (ΔH_{cc})

Although crystallinity decreased with the addition of CNFL, CNFL had a positive effect on the thermal stability of the CNFL-filled PLA composite films (Fig. 5). The maximum degradation temperature of the composites, determined from the peak temperature of the derivative curves, was very similar to that of the pure PLA film. Considering that the maximum degradation temperature of CNFL is 362 °C, this consistency in thermal stability is reasonable. Additionally, the initiation of thermal degradation was delayed with the addition of CNFL, as shown in the increased $T_{d5\%}$. This may be attributed to the enhanced cold crystallization (Wang *et al.* 2015).

Further confirmation of thermal stability was obtained by analyzing the LCTE, measured by a thermal mechanical analyzer (TA Instruments). Whereas the LCTE of the composite films showed similar values of 80 to 90 ppm/°C below T_g, the LCTE above T_g significantly decreased with the addition of CNFL (Fig. 6). This phenomenon could be related to the increased cold crystallization of PLA in the composite upon addition of CNFL. Above T_g, the PLA in the composite film further crystallized, enhancing elastic properties and strength, because crystalline regions provide a more rigid, ductile, and structured matrix that better resists deformation and mechanical stress (Gupta and Kumar 2007; Simmons *et al.* 2019; Cao *et al.* 2019). Additionally, uniformly dispersed CNFLs in the PLA matrix likely acted as scaffolds, efficiently suppressing the deformation of PLA polymers at the higher temperature, thereby enhancing the dimensional and thermal stability of the composite films. The enhanced thermal stability demonstrated the potential application of CNFL-filled PLA composite films for high-temperature operations, as well as the possibility of tuning thermal stability by controlling the addition of CNFL.

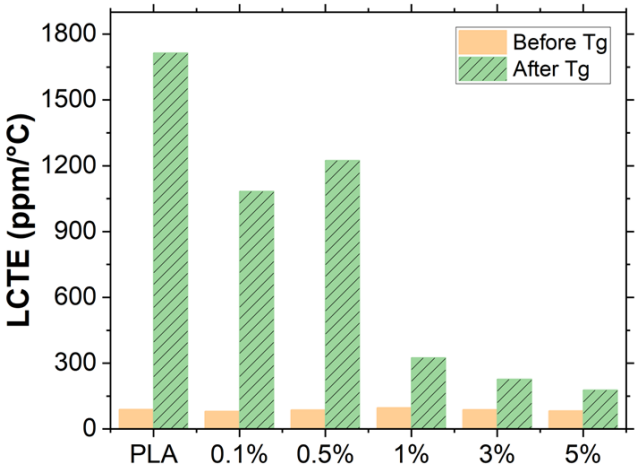

Fig. 6. Linear coefficient of thermal expansion (LCTE) of CNFL-filled PLA composite films with CNFL loading ratios of 0.1%, 0.5%, 1%, 3%, and 5%.

Oxygen barrier properties of CNFL-filled PLA composite films

Oxygen barrier properties were determined by measuring the oxygen transmission rate using an oxygen analyzer. The thickness of the composite films varied; thus, oxygen permeability was calculated *via* multiplication of the oxygen transmission rate by the thickness (Table 3).

Table 3. Thickness, Oxygen Transmission Rate, and Oxygen Permeability of CNFL-Filled PLA Composite Films

	Thickness (μm)	Oxygen Transmission Rate ($cm^3/m^2/day$)	Oxygen Permeability ($cm^3mm/m^2/day/atm$)
PLA	38	880	33.0
0.5 %	27	610	16.3
1 %	53	270	14.1
3 %	45	448	19.9
5 %	42	409	17.0

Although the oxygen permeability of pure PLA film was 33.0 $cm^3mm/m^2/day/atm$, the addition of 0.5% CNFL reduced the oxygen permeability to 16.3 $cm^3mm/m^2/day/atm$, effectively halving this value. The lowest oxygen permeability was achieved with 1% CNFL addition, after which the permeability showed a slight increasing trend. Initially, the disc-like structure of CNFL increases the tortuosity within the composite films, enhancing the complexity and length of the oxygen penetration path. However, when the amount of CNFL exceeds a certain threshold (1% in this study), CNFL might flocculate in the composite films, increasing oxygen permeability. Therefore, further research concerning CNFL loading optimization is necessary. Nevertheless, the permeability remained lower than that of pure PLA film.

This study comprehensively investigated the effect of disc-type nanofiller CNFL on PLA composite films, focusing on their mechanical, thermal, and oxygen barrier properties. PLA, a bio-based plastic, is widely used as a food packaging material due to its biocompatibility and derivation from renewable resources. While its water and oxygen barrier properties are sufficient for short-term use, such as disposable drink packaging, its

oxygen barrier properties and brittleness still need improvement for long-term applications (Ehman and Area 2021; Sombatsompop *et al.* 2021; Mohan and Panneerselvam 2022; Lee *et al.* 2024). The incorporation of CNFL significantly enhanced the mechanical properties of the PLA composite films, resulting in increased strength and stiffness along with stable flexibility, in agreement with previous studies (Zhang *et al.* 2014; Nasrin *et al.* 2017; Hassan and Koyama 2020). Additionally, CNFL improved the thermal dimensional stability and oxygen barrier properties of the composites, which contrasts with the decreased thermal stability reported in a previous study (Hassan and Koyama 2020), indicating the superior properties of chitin nanoflakes over microparticles These findings suggest that CNFL-filled PLA composite films exhibit considerable potential for applications as renewable and safe packaging materials due to their superior oxygen barrier properties and enhanced mechanical performance while retaining the existing benefits of PLA. These attributes make them ideal for protecting sensitive products, such as food and pharmaceuticals, from oxidative degradation, thereby extending shelf life and maintaining quality. Future research should address long-term stability, biodegradability, optimization of CNFL loading, and commercial scalability to further establish these composites as versatile and sustainable materials for various advanced applications.

CONCLUSIONS

1. Chitin-derived nanoflakes (CNFL)-filled poly(lactic acid) (PLA) composite films exhibited enhanced mechanical properties, including increased strength and stiffness along with stable flexibility, making them suitable for various packaging applications.
2. CNFL acted as a nucleating agent, increasing the crystallinity of PLA and ultimately improving the mechanical properties of CNFL-filled PLA composites.
3. The thermal stability of PLA composite films was improved by incorporating CNFL as a filler, which suppressed the thermal deformation of PLA, especially at high temperatures.
4. The incorporation of chitin nanofiller (CNFL) into PLA significantly reduced oxygen permeability, demonstrating its better oxygen-barrier properties.
5. CNFL-filled PLA composite films offer significant advantages as renewable and safe packaging materials, particularly for protecting sensitive products from oxygen degradation.

ACKNOWLEDGMENTS

This work was supported by research fund of Chungnam National University

REFERENCES CITED

Aklog, Y. F., Egusa, M., Kaminaka, H., Izawa, H., Morimoto, M., Saimoto, H., and Ifuku, S. (2016). "Protein/$CaCO_3$/chitin nanofiber complex prepared from crab shells by simple mechanical treatment and its effect on plant growth," *International Journal*

of Molecular Sciences 17(10), article 1600. DOI: 10.3390/ijms17101600

ASTM D3418 (2021). "Standard test method for transition temperatures and enthalpies of fusion and crystallization of polymers by differential scanning," ASTM International, West Conshohocken, PA, USA.

ASTM D3985 (2017). "Standard test method for oxygen gas transmission rate through plastic film and sheeting using a coulometric sensor," ASTM International, West Conshohocken, PA, USA.

Bai, L., Liu, L., Esquivel, M., Tardy, B. L., Huan, S., Niu, X., Liu, S., Yang, G., Fan, Y., and Rojas, O. J. (2022). "Nanochitin: Chemistry, structure, assembly, and applications," *Chemical Reviews* 122(13), 11604-11674. DOI: 10.1021/acs.chemrev.2c00125

Battegazzore, D., Alongi, J., and Frache, A. (2014). "Poly(lactic acid)-based composites containing natural fillers: Thermal, mechanical and barrier properties," *Journal of Polymers and the Environment* 22(1), 88-98. DOI: 10.1007/s10924-013-0616-9

Cao, Z.-W., Pan, H.-W., Chen, Y.-J., Bian, J.-J., Han, L.-J., Zhang, H.-L., Dong, L.-S., and Yang, Y.-M. (2019). "Transform poly (lactic acid) packaging film from brittleness to toughness using traditional industrial equipments," *Polymer* 180, article 121728. DOI: 10.1016/j.polymer.2019.121728

Cárdenas, G., Cabrera, G., Taboada, E., and Miranda, S. P. (2004). "Chitin characterization by SEM, FTIR, XRD, and 13C cross polarization/mass angle spinning NMR," *Journal of Applied Polymer Science* 93(4), 1876-1885. DOI: 10.1002/app.20647

Civancik-Uslu, D., Ferrer, L., Puig, R., and Fullana-i-Palmer, P. (2018). "Are functional fillers improving environmental behavior of plastics? A review on LCA studies," *Science of The Total Environment* 626, 927-940. DOI: 10.1016/j.scitotenv.2018.01.149

Cui, Y., Kumar, S., Kona, B. R., and Houcke, D. van. (2015). "Gas barrier properties of polymer/clay nanocomposites," *RSC Advances* 5(78), 63669-63690. DOI: 10.1039/C5RA10333A

Dahmane, E. M., Taourirte, M., Eladlani, N., and Rhazi, M. (2014). "Extraction and characterization of chitin and chitosan from *Parapenaeus longirostris* from Moroccan local sources," *International Journal of Polymer Analysis and Characterization* 19(4), 342-351. DOI: 10.1080/1023666X.2014.902577

Ehman, N., and Area, M. (2021). "Bioplastics are revolutionizing the packaging industry," *BioResources* 16(3), 4663-4666. DOI: 10.15376/biores.16.3.4663-4666

Fan, Y., Saito, T., and Isogai, A. (2010). "Individual chitin nano-whiskers prepared from partially deacetylated α-chitin by fibril surface cationization," *Carbohydrate Polymers* 79(4), 1046-1051. DOI: 10.1016/j.carbpol.2009.10.044

FAO. (2014). "The State of World Fisheries and Aquaculture 2014 (SOFIA)," Food and Agriculture Organization of the United Nations.

Fernández-Marín, R., Morales, A., Erdocia, X., Iturrondobeitia, M., Labidi, J., and Lizundia, E. (2024). "Chitosan–chitin nanocrystal films from lobster and spider crab: Properties and environmental sustainability," *ACS Sustainable Chemistry & Engineering*. DOI: 10.1021/acssuschemeng.4c01205

Fiore, V., Botta, L., Scaffaro, R., Valenza, A., and Pirrotta, A. (2014). "PLA based biocomposites reinforced with Arundo donax fillers," *Composites Science and Technology* 105, 110-117. DOI: 10.1016/j.compscitech.2014.10.005

Focher, B., Naggi, A., Torri, G., Cosani, A., and Terbojevich, M. (1992). "Structural differences between chitin polymorphs and their precipitates from solutions—Evidence from CP-MAS 13C-NMR, FT-IR and FT-Raman spectroscopy," *Carbohydrate Polymers* 17(2), 97-102. DOI: 10.1016/0144-8617(92)90101-U

Foreman, J., Sauerbrunn, S. R., and Marcozzi, C. L. (2011). "Investigating the sensitivity of thermal analysis methods to glass transition," *International Polymer Science and Technology* 38(6), T29-T36.

Francesko, A., Díaz González, M., Lozano, G. R., and Tzanov, T. (2010). "12 - Developments in the processing of chitin, chitosan and bacterial cellulose for textile and other applications," in: *Advances in Textile Biotechnology*, V. A. Nierstrasz and A. Cavaco-Paulo (eds.), Woodhead Publishing, pp. 288-311. DOI: 10.1533/9780857090232.2.288

Gao, P., Muller, S. E., Chun, J., Zhong, L., and Kennedy, Z. C. (2023). "Effects of 2D filler on rheology of additive manufacturing polymers: Simulation and experiment on polyetherketoneketone-mica composites," *Polymer* 269, 125722. DOI: 10.1016/j.polymer.2023.125722

Geyer, R. (2020a). "A brief history of plastics," in: *Mare Plasticum - The Plastic Sea: Combatting Plastic Pollution Through Science and Art*, M. Streit-Bianchi, M. Cimadevila, and W. Trettnak (eds.), Springer International Publishing, Cham, pp. 31-47. DOI: 10.1007/978-3-030-38945-1_2

Geyer, R. (2020b). "Chapter 2 - Production, use, and fate of synthetic polymers," in: *Plastic Waste and Recycling*, T. M. Letcher (ed.), Academic Press, pp. 13-32. DOI: 10.1016/B978-0-12-817880-5.00002-5

Goodrich, J. D., and Winter, W. T. (2007). "α-Chitin nanocrystals prepared from shrimp shells and their specific surface area measurement," *Biomacromolecules* 8(1), 252-257. DOI: 10.1021/bm0603589

Gupta, A. P., and Kumar, V. (2007). "New emerging trends in synthetic biodegradable polymers – Polylactide: A critique," *European Polymer Journal* 43(10), 4053-4074. DOI: 10.1016/j.eurpolymj.2007.06.045

Han, J., Kwon, S., Kim, S. Y., and Oh, K. (2024). "Chitin/calcium carbonate complex microparticles and their effects on polylactic acid composite films," *Cellulose*. DOI: 10.1007/s10570-024-05967-w

Hasan, S., Boddu, V. M., Viswanath, D. S., and Ghosh, T. K. (2022). "The structural difference between chitin and chitosan," in: *Chitin and Chitosan: Science and Engineering*, S. Hasan, V. M. Boddu, D. S. Viswanath, and T. K. Ghosh (eds.), Springer International Publishing, Cham, pp. 79-102. DOI: 10.1007/978-3-031-01229-7_4

Hassan, M. M., and Koyama, K. (2020). "Thermomechanical and viscoelastic properties of green composites of PLA using chitin micro-particles as fillers," *Journal of Polymer Research* 27(2), 27. DOI: 10.1007/s10965-019-1991-2

Hasegawa, T. (2017). "Infrared spectroscopy as a vibrational spectroscopy," in: *Quantitative Infrared Spectroscopy for Understanding of a Condensed Matter*, T. Hasegawa (ed.), Springer Japan, Tokyo, pp. 1-36. DOI: 10.1007/978-4-431-56493-5_1

Hatta, H., Taya, M., Kulacki, F. A., and Harder, J. F. (1992). "Thermal diffusivities of composites with various types of filler," *Journal of Composite Materials* 26(5), 612-625. DOI: 10.1177/002199839202600501

Hou, J., Aydemir, B. E., and Dumanli, A. G. (2021). "Understanding the structural diversity of chitins as a versatile biomaterial," *Philosophical Transactions of the Royal Society A: Mathematical, Physical and Engineering Sciences* 379(2206), article 20200331. DOI: 10.1098/rsta.2020.0331

Hubbe, M. A., and Grigsby, W. (2020). "From nanocellulose to wood particles: A review of particle size *vs*. the properties of plastic composites reinforced with cellulose-based entities," *BioResources* 15(1), 2030-2081. DOI: 10.15376/biores.15.1.2030-2081

Hubbe, M. A., Lavoine, N., Lucia, L. A., and Dou, C. (2021). "Formulating bioplastic composites for biodegradability, recycling, and performance: A review," *BioResources* 16(1), 2021-2083. DOI: 10.15376/biores.16.1.Hubbe

Ifuku, S., Morooka, S., Morimoto, M., and Saimoto, H. (2010). "Acetylation of chitin nanofibers and their transparent nanocomposite films," *Biomacromolecules* 11(5), 1326-1330. DOI: 10.1021/bm100109a

Islam, Md. R., Rashid, Md. N., Dev, B., Sayeed, Md. Y., Alam, Md. R., Mahmud, R. U., and Rahman, M. Z. (2024). "13.25 - Progress in sustainable applications of polymers and biopolymers," in: *Comprehensive Materials Processing (Second Edition),* S. Hashmi (ed.), Elsevier, Oxford, pp. 523-554. DOI: 10.1016/B978-0-323-96020-5.00212-0

Joseph Arockiam, A., Karthikeyan Subramanian, Padmanabhan, R. G., Rajeshkumar Selvaraj, Dilip Kumar Bagal, and Rajesh, S. (2022). "A review on PLA with different fillers used as a filament in 3D printing," *Materials Today: Proceedings* 50, 2057-2064. DOI: 10.1016/j.matpr.2021.09.413

Kameda, T., Miyazawa, M., Ono, H., and Yoshida, M. (2005). "Hydrogen bonding structure and stability of α-chitin studied by 13C solid-state NMR," *Macromolecular Bioscience* 5(2), 103-106. DOI: 10.1002/mabi.200400142

Kane, S., Van Roijen, E., Ryan, C., and Miller, S. (2022). "Reducing the environmental impacts of plastics while increasing strength: Biochar fillers in biodegradable, recycled, and fossil-fuel derived plastics," *Composites Part C: Open Access* 8, article 100253. DOI: 10.1016/j.jcomc.2022.100253

Karim, N., Sarker, F., Afroj, S., Zhang, M., Potluri, P., and Novoselov, K. S. (2021). "Sustainable and multifunctional composites of graphene-based natural jute fibers," *Advanced Sustainable Systems* 5(3), article 2000228. DOI: 10.1002/adsu.202000228

Kiziltas, A., Liu, W., Tamrakar, S., and Mielewski, D. (2021). "Graphene nanoplatelet reinforcement for thermal and mechanical properties enhancement of bio-based polyamide 6, 10 nanocomposites for automotive applications," *Composites Part C: Open Access* 6, article 100177. DOI: 10.1016/j.jcomc.2021.100177

Korol, J., Burchart-Korol, D., and Pichlak, M. (2016). "Expansion of environmental impact assessment for eco-efficiency evaluation of biocomposites for industrial application," *Journal of Cleaner Production* 113, 144-152. DOI: 10.1016/j.jclepro.2015.11.101

Kumar, C. M., Ashok, R. B., Kumar, M., and Roopa, C. P. (2022). "Natural nano-fillers materials for the bio-composites: A review," *Journal of the Indian Chemical Society* 99(10), article 100715. DOI: 10.1016/j.jics.2022.100715

Kumar Patel, K., and Purohit, R. (2019). "Improved shape memory and mechanical properties of microwave-induced thermoplastic polyurethane/graphene nanoplatelets composites," *Sensors and Actuators A: Physical* 285, 17-24. DOI: 10.1016/j.sna.2018.10.049

Lee, B., Son, I., Kim, J. H., Yoo, J. Y., Kim, C., Cho, C. H., Moon, G., and Lee, J. H. (2018). "Improvement of adhesive strength and moisture barrier property of UV/heat dual-curable sealant for liquid crystal display by inclusion of inorganic plate-type filler," *Molecular Crystals and Liquid Crystals* 660(1), 150-155. DOI: 10.1080/15421406.2018.1456142

Lee, Y. J., Lim, D. G., Cha, J. E., Lee, D. Y., Lee, T.-J., and Kim, H. J. (2024). "Barrier properties of polyhydroxybutyrate/ethyl cellulose-blend-coated paper through the incorporation of organo-modified nanoclay as a coating component," *BioResources* 19(3), 4782-4799.

Lezak, E., Kulinski, Z., Masirek, R., Piorkowska, E., Pracella, M., and Gadzinowska, K. (2008). "Mechanical and thermal properties of green polylactide composites with natural fillers," *Macromolecular Bioscience* 8(12), 1190-1200. DOI: 10.1002/mabi.200800040

Liu, L., Seta, F. T., An, X., Yang, J., Zhang, W., Dai, H., Cao, H., Xu, Q., and Liu, H. (2020). "Facile isolation of colloidal stable chitin nano-crystals from *Metapenaeus ensis* shell *via* solid maleic acid hydrolysis and their application for synthesis of silver nanoparticles," *Cellulose* 27(17), 9853-9875. DOI: 10.1007/s10570-020-03499-7

Lizundia, E., Petisco, S., and Sarasua, J.-R. (2013). "Phase-structure and mechanical properties of isothermally melt-and cold-crystallized poly (L-lactide)," *Journal of the Mechanical Behavior of Biomedical Materials* 17, 242-251. DOI: 10.1016/j.jmbbm.2012.09.006

Lu, Y., Sun, Q., She, X., Xia, Y., Liu, Y., Li, J., and Yang, D. (2013). "Fabrication and characterisation of α-chitin nanofibers and highly transparent chitin films by pulsed ultrasonication," *Carbohydrate Polymers* 98(2), 1497-1504. DOI: 10.1016/j.carbpol.2013.07.038

Mahmoud Zaghloul, M. Y., Yousry Zaghloul, M. M., and Yousry Zaghloul, M. M. (2021). "Developments in polyester composite materials – An in-depth review on natural fibres and nano fillers," *Composite Structures* 278, article 114698. DOI: 10.1016/j.compstruct.2021.114698

Martin, O., and Avérous, L. (2001). "Poly(lactic acid): Plasticization and properties of biodegradable multiphase systems," *Polymer* 42(14), 6209-6219. DOI: 10.1016/S0032-3861(01)00086-6

Mohan, S., and Panneerselvam, K. (2022). "A short review on mechanical and barrier properties of polylactic acid-based films.," *Materials Today: Proceedings* 56, 3241-3246. DOI: 10.1016/j.matpr.2021.09.375

Nasrin, R., Biswas, S., Rashid, T. U., Afrin, S., Jahan, R. A., Haque, P., and Rahman, M. M. (2017). "Preparation of Chitin-PLA laminated composite for implantable application," *Bioactive materials* 2(4), 199-207. DOI: 10.1016/j.bioactmat.2017.09.003

Nikolov, S., Fabritius, H., Petrov, M., Friák, M., Lymperakis, L., Sachs, C., Raabe, D., and Neugebauer, J. (2011). "Robustness and optimal use of design principles of arthropod exoskeletons studied by ab initio-based multiscale simulations," *Journal of the Mechanical Behavior of Biomedical Materials* 4(2), 129-145. DOI: 10.1016/j.jmbbm.2010.09.015

Ogawa, Y., Kimura, S., Wada, M., and Kuga, S. (2010). "Crystal analysis and high-resolution imaging of microfibrillar α-chitin from *Phaeocystis*," *Journal of Structural Biology* 171(1), 111-116. DOI: 10.1016/j.jsb.2010.03.010

Ouchiar, S., Stoclet, G., Cabaret, C., and Gloaguen, V. (2016). "Influence of the filler nature on the crystalline structure of polylactide-based nanocomposites: New insights into the nucleating effect," *Macromolecules* 49(7), 2782-2790. DOI: 10.1021/acs.macromol.5b02746

Oun, A. A., and Rhim, J.-W. (2018). "Effect of isolation methods of chitin nanocrystals on the properties of chitin-silver hybrid nanoparticles," *Carbohydrate Polymers* 197, 349-358. DOI: 10.1016/j.carbpol.2018.06.033

Papageorgiou, G. Z., Achilias, D. S., Nanaki, S., Beslikas, T., and Bikiaris, D. (2010). "PLA nanocomposites: Effect of filler type on non-isothermal crystallization," *Thermochimica Acta* 511(1), 129-139. DOI: 10.1016/j.tca.2010.08.004

Ravi Kumar, M. N. V. (2000). "A review of chitin and chitosan applications," *Reactive and Functional Polymers* 46(1), 1-27. DOI: 10.1016/S1381-5148(00)00038-9

Rinaudo, M. (2006). "Chitin and chitosan: Properties and applications," *Progress in Polymer Science* 31(7), 603-632. DOI: 10.1016/j.progpolymsci.2006.06.001

Jani, S. P., Sujin, J. A., Rajaganapathy, C., and Khan, A. (2024). "Development of hybrid composite with natural fillers for mechanical property and machinability study," *Progress in Rubber, Plastics and Recycling Technology* 40(1), 17-32. DOI: 10.1177/14777606231186633

Shakoor, A., and Thomas, N. l. (2014). "Talc as a nucleating agent and reinforcing filler in poly(lactic acid) composites," *Polymer Engineering & Science* 54(1), 64-70. DOI: 10.1002/pen.23543

Shen, X., Zheng, Q., and Kim, J.-K. (2021). "Rational design of two-dimensional nanofillers for polymer nanocomposites toward multifunctional applications," *Progress in Materials Science* 115, article 100708. DOI: 10.1016/j.pmatsci.2020.100708

Simmons, H., Tiwary, P., Colwell, J. E., and Kontopoulou, M. (2019). "Improvements in the crystallinity and mechanical properties of PLA by nucleation and annealing," *Polymer Degradation and Stability* 166, 248-257. DOI: 10.1016/j.polymdegradstab.2019.06.001

Sombatsompop, N., Srimalanon, P., Markpin, T., and Prapagdee, B. (2021). "Polylactic Acid (PLA): Improve It, Use It, and Dump It Faster," *BioResources* 16(2), 2196-2199. DOI: 10.15376/biores.16.2.2196-2199

Tan, B., and Thomas, N. L. (2016). "A review of the water barrier properties of polymer/clay and polymer/graphene nanocomposites," *Journal of Membrane Science* 514, 595-612. DOI: 10.1016/j.memsci.2016.05.026

Tanaka, K., Yamamoto, K., and Kadokawa, J. (2014). "Facile nanofibrillation of chitin derivatives by gas bubbling and ultrasonic treatments in water," *Carbohydrate Research* 398, 25-30. DOI: 10.1016/j.carres.2014.08.008

Tran, T. H., Nguyen, H.-L., Hao, L. T., Kong, H., Park, J. M., Jung, S.-H., Cha, H. G., Lee, J. Y., Kim, H., Hwang, S. Y., Park, J., and Oh, D. X. (2019). "A ball milling-based one-step transformation of chitin biomass to organo-dispersible strong nanofibers passing highly time and energy consuming processes," *International Journal of Biological Macromolecules* 125, 660-667. DOI: 10.1016/j.ijbiomac.2018.12.086

Usman, C., Mabrouk, A., and Abdala, A. (2022). "Thermally enhanced polyethylene nanocomposites for polymer heat exchanger applications," in: *Sustainable Energy-Water-Environment Nexus in Deserts*, E. Heggy, V. Bermudez, and M. Vermeersch, (eds.), Springer International Publishing, Cham, 227-232. DOI: 10.1007/978-3-030-76081-6_27

Wang, L., Wang, Y., Huang, Z., and Weng, Y. (2015). "Heat resistance, crystallization behavior, and mechanical properties of polylactide/nucleating agent composites," *Materials & Design (1980-2015)* 66, 7-15. DOI: 10.1016/j.matdes.2014.10.011

Wei, A., Fu, J., and Guo, F. (2021). "Mechanical properties of chitin polymorphs: A computational study," *Journal of Materials Science* 56(20), 12048-12058. DOI: 10.1007/s10853-021-06086-8

Wootthikanokkhan, J., Cheachun, T., Sombatsompop, N., Thumsorn, S., Kaabbuathong, N., Wongta, N., Wong-On, J., Na Ayutthaya, S. I., and Kositchaiyong, A. (2013). "Crystallization and thermomechanical properties of PLA composites: Effects of additive types and heat treatment," *Journal of Applied Polymer Science* 129(1), 215-223. DOI: 10.1002/app.38715

Yadav, R., Singh, M., Shekhawat, D., Lee, S.-Y., and Park, S.-J. (2023). "The role of fillers to enhance the mechanical, thermal, and wear characteristics of polymer composite materials: A review," *Composites Part A: Applied Science and Manufacturing* 175, article 107775. DOI: 10.1016/j.compositesa.2023.107775

Yan, N., and Chen, X. (2015). "Sustainability: Don't waste seafood waste," *Nature* 524(7564), 155-157. DOI: 10.1038/524155a

Yi, M., Shen, Z., Zhang, W., Zhu, J., Liu, L., Liang, S., Zhang, X., and Ma, S. (2013). "Hydrodynamics-assisted scalable production of boron nitride nanosheets and their application in improving oxygen-atom erosion resistance of polymeric composites," *Nanoscale* 5(21), 10660-10667. DOI: 10.1039/C3NR03714B

Yu, Y.-H., Lin, Y.-Y., Lin, C.-H., Chan, C.-C., and Huang, Y.-C. (2013). "High-performance polystyrene/graphene-based nanocomposites with excellent anti-corrosion properties," *Polymer Chemistry* 5(2), 535-550. DOI: 10.1039/C3PY00825H

Yuan, Y., Chesnutt, B. M., Haggard, W. O., and Bumgardner, J. D. (2011). "Deacetylation of chitosan: Material characterization and *in vitro* evaluation *via* albumin adsorption and pre-osteoblastic cell cultures," *Materials* 4(8), 1399-1416. DOI: 10.3390/ma4081399

Yuan, Y., Hong, S., Lian, H., Zhang, K., and Liimatainen, H. (2020). "Comparison of acidic deep eutectic solvents in production of chitin nanocrystals," *Carbohydrate Polymers* 236, article 116095. DOI: 10.1016/j.carbpol.2020.116095

Zhang, Q., Wei, S., Huang, J., Feng, J., and Chang, P. R. (2014). "Effect of surface acetylated-chitin nanocrystals on structure and mechanical properties of poly(lactic acid)," *Journal of Applied Polymer Science* 131(2). DOI: 10.1002/app.39809

Zhang, X., Shi, J., Zhou, J., and Nan, J. (2022). "Nucleation effect of cellulose nanocrystals/polybutylene succinate composite filler on polylactic acid/polybutylene succinate blends," *Polymer Bulletin* 79(7), 5481-5494. DOI: 10.1007/s00289-021-03567-3

Zhang, Y., Zhang, T., Kuga, S., Wu, M., and Huang, Y. (2020). "Polarities-induced weakening of molecular interaction and formation of nanocellulose with different dimensions," *ACS Sustainable Chemistry & Engineering* 8(25), 9277-9290. DOI: 10.1021/acssuschemeng.0c00464

Zhao, M., Kuga, S., Jiang, S., Wu, M., and Huang, Y. (2016). "Cellulose nanosheets induced by mechanical impacts under hydrophobic environment," *Cellulose* 23(5), 2809-2818. DOI: 10.1007/s10570-016-1033-8

Z. Naser, A., Deiab, I., and M. Darras, B. (2021). "Poly(lactic acid) (PLA) and polyhydroxyalkanoates (PHAs), green alternatives to petroleum-based plastics: A review," *RSC Advances* 11(28), 17151-17196. DOI: 10.1039/D1RA02390J

Article submitted: July 15, 2024; Peer review completed: August 1, 2024; Revised version received and accepted: August 8, 2024; Published: August 16, 2024.
DOI: 10.15376.biores.19.4.7216-7238

APPENDIX

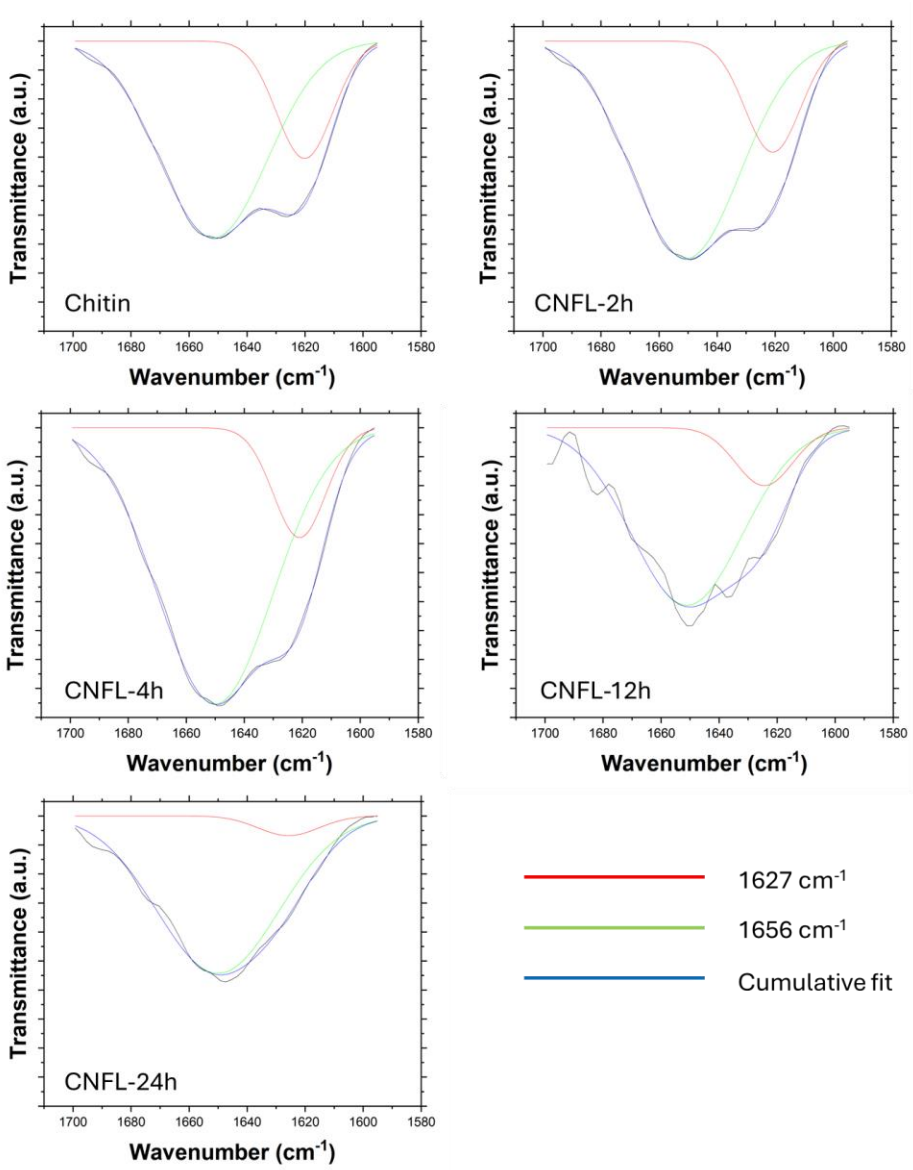

Fig. A1. Deconvolution of the 1627 cm^{-1} and 1656 cm^{-1} peaks

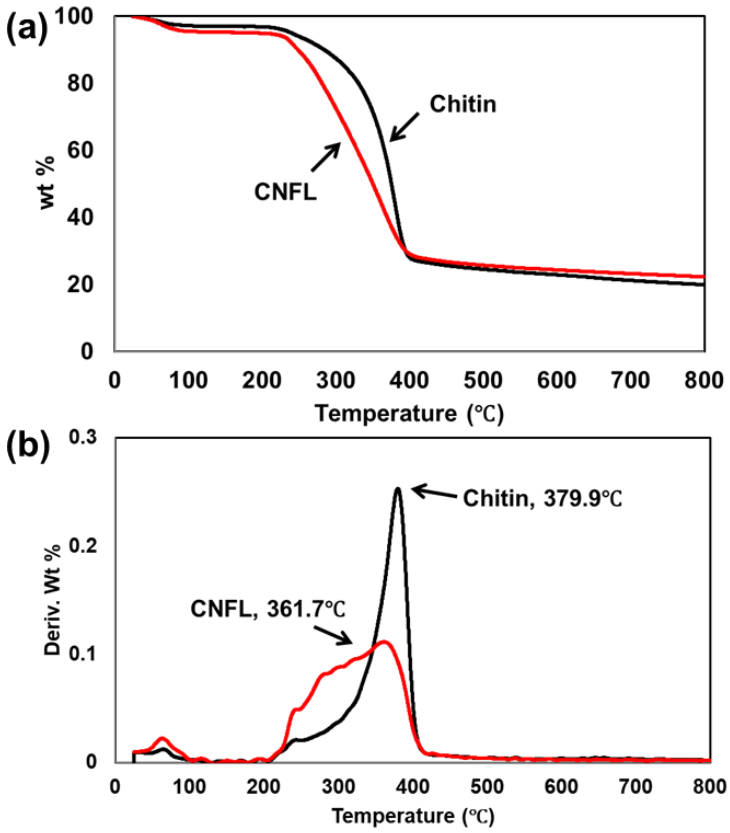

Fig. A2. Thermogravimetric analysis curves (a, b) of chitin and chitin-derived nanoflake/s (CNFL-4h). (b) Derivative thermogravimetric curves from (a).

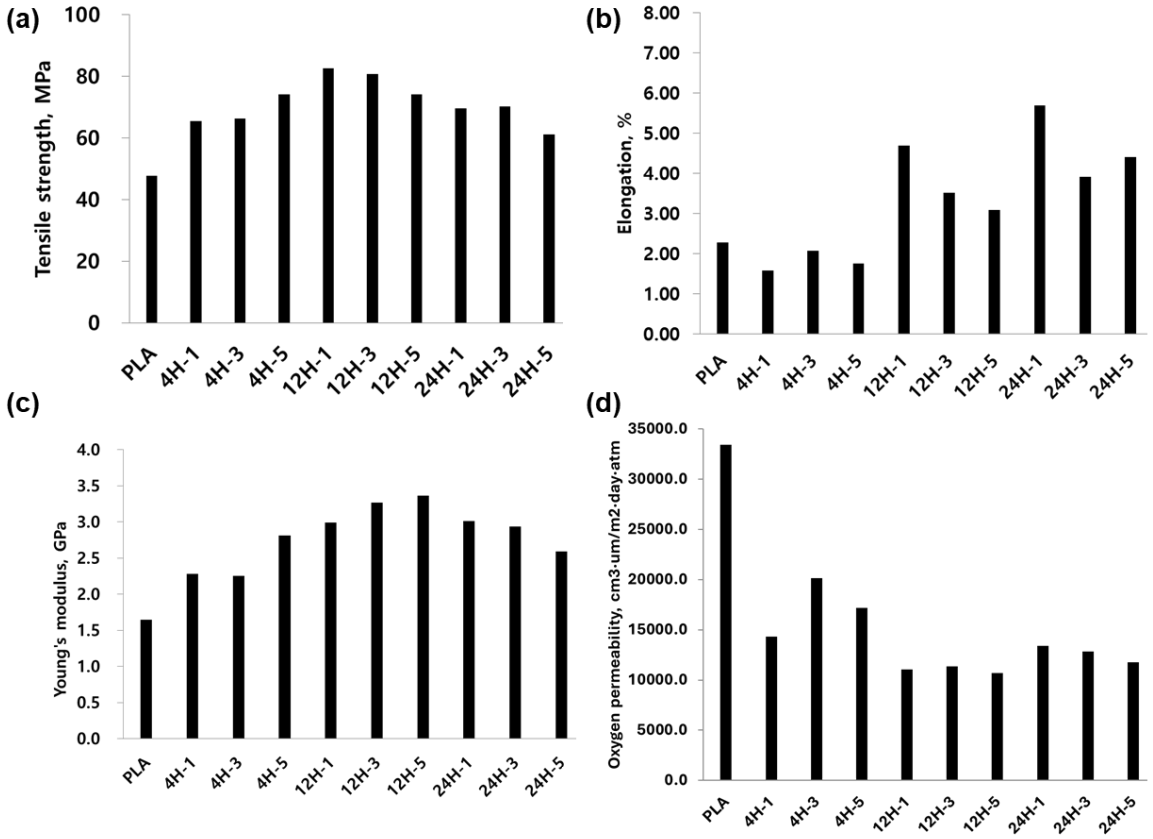

Fig. A3. Tensile properties (a-c) and oxygen permeability (d) of CNFL-filled polylactic acid (PLA) composites with CNFL loading ratios of 1%, 3%, and 5% and different CNFL ball milling times (4H, 12H, and 24H). Tensile properties of the composite films: (a) tensile stress, (b) elongation at break (%), and (c) Young's modulus